Science Advances
AAAS

advances.sciencemag.org/cgi/content/full/6/20/eaax3868/DC1

Supplementary Materials for

The RNA binding protein CPEB2 regulates hormone sensing in mammary gland development and luminal breast cancer

Rosa Pascual, Judit Martín, Fernando Salvador, Oscar Reina, Veronica Chanes, Alba Millanes-Romero, Clara Suñer, Gonzalo Fernández-Miranda, Anna Bartomeu, Yi-Shuian Huang, Roger R. Gomis, Raúl Méndez*,

*Corresponding author. Email: raul.mendez@irbbarcelona.org

Published 15 May 2020, *Sci. Adv.* **6**, eaax3868 (2020)
DOI: 10.1126/sciadv.aax3868

The PDF file includes:

Figs. S1 to S11

Other Supplementary Material for this manuscript includes the following:

(available at advances.sciencemag.org/cgi/content/full/6/20/eaax3868/DC1)

Tables S1 and S2

Supplementary Fig. 1

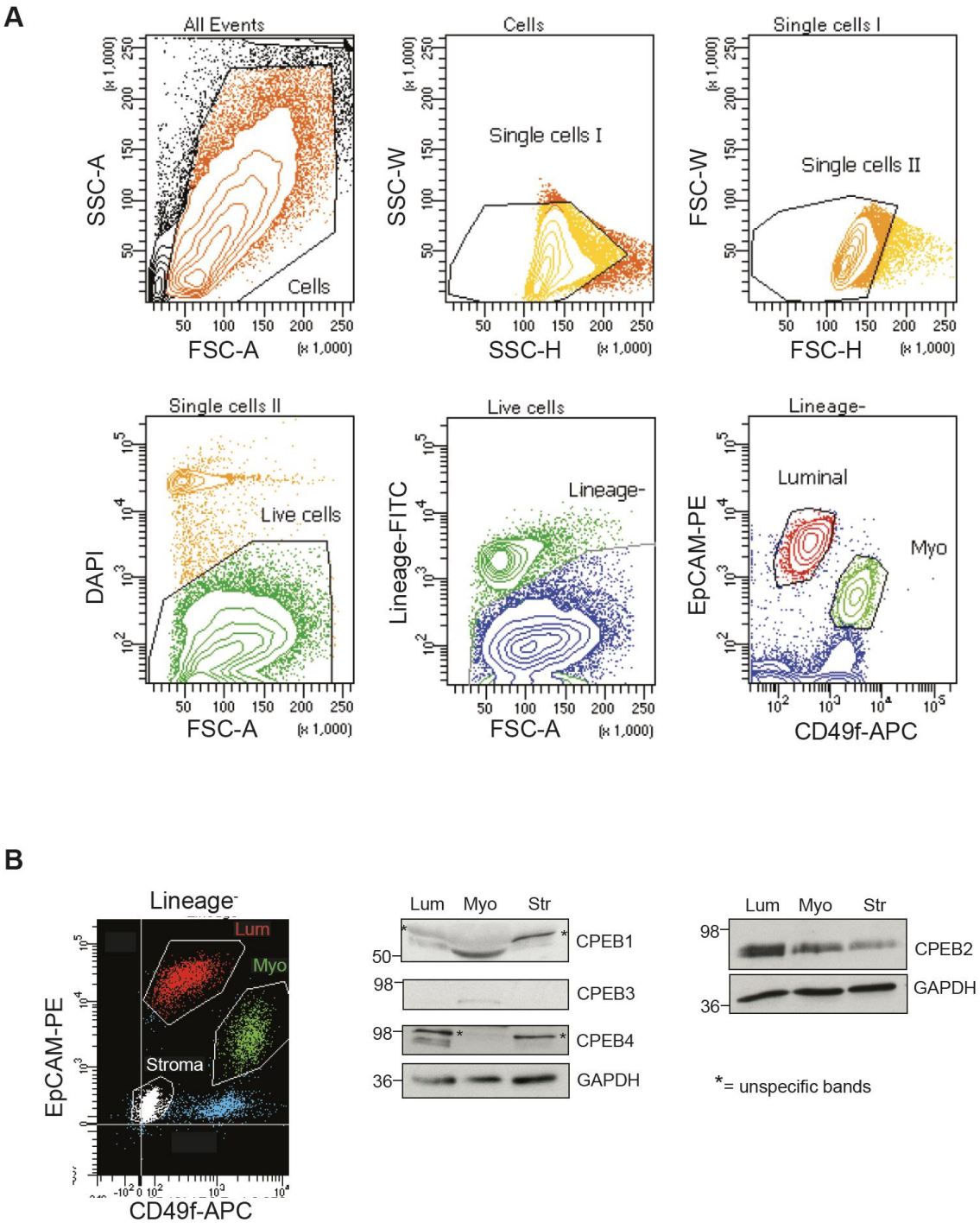

Supplementary Fig.1. Expression of the CPEB1-4 in mammary epithelial and stromal cells. (A) FACS strategy. Representative FACS plots showing the gating strategy for isolation and analysis of luminal (EpCAM^{high}CD49f^{low}) and myoepithelial (EpCAMlowCD49fhigh) populations of the mammary tissue. Lineage staining includes immune (CD45+), endothelial (CD31+) and erythroid (Ter119+) populations. (B) FACS plot of the sorted populations (left) and western-blot detection (right) of murine CPEB1-4 in luminal (Lum), myoepithelial (Myo) and stromal (Str) cell populations. GAPSH is used as a loading control.

Supplementary Fig. 2

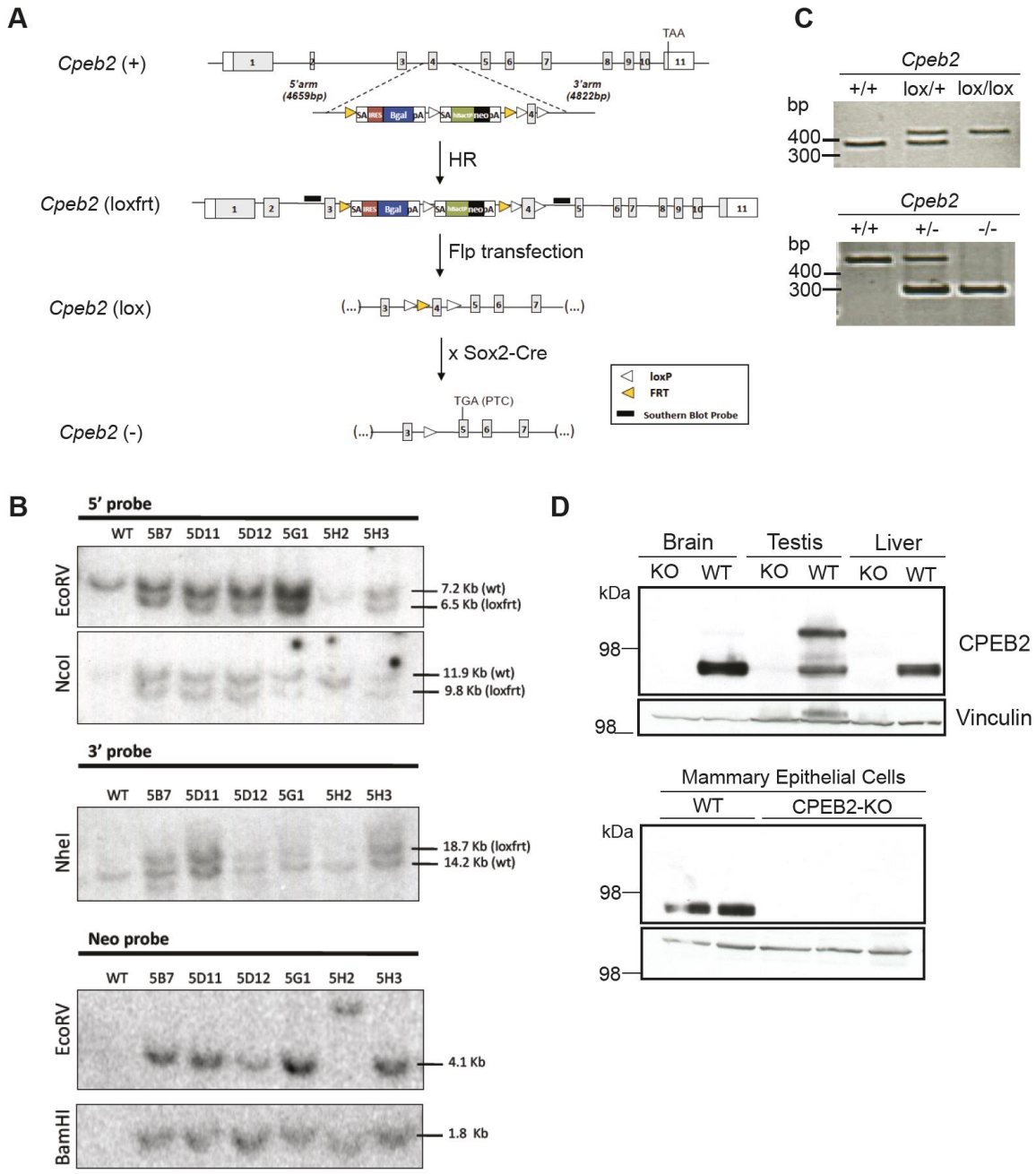

Supplementary Fig.2. Generation of CPEB2 KO mouse model. (A) Schematic view of the targeting strategy by homologous recombination (HR) at the *Cpeb2* locus in mouse embryonic stem (ES) cells. The *Cpeb2* locus in *Mus musculus* contains 11 exons (boxes), including protein-coding (grey) and untranslated (clear) sequences. Also loxP and FRT sites are depicted. The neo cassette was deleted by expressing Flp recombinase in vitro. To obtain excision of exon4 and loss of CPEB2 ubiquitously, mice were crossed with Sox2-Cre mice. hBactP, promoter. Bgal, beta-galactosidase. Neo, neomycin. PTC, premature termination codon. IRES, internal ribosome entry site. SA, splicing acceptor. pA, polyA sequence. (B) ES clones that underwent HR assessed by Southern Blotting. DNA was digested with the indicated restriction enzymes and hybridized with the 5', 3' or Neo probes as indicated in (A). (C) PCR amplification for either conditional (upper panel) or null (lower panel) Cpeb2 alleles. (D) Extracts from whole tissue or isolated MECs from WT and constitutive KO mice assessed by western blotting for CPEB2 and Vinculin (loading control).

Supplementary Fig. 3

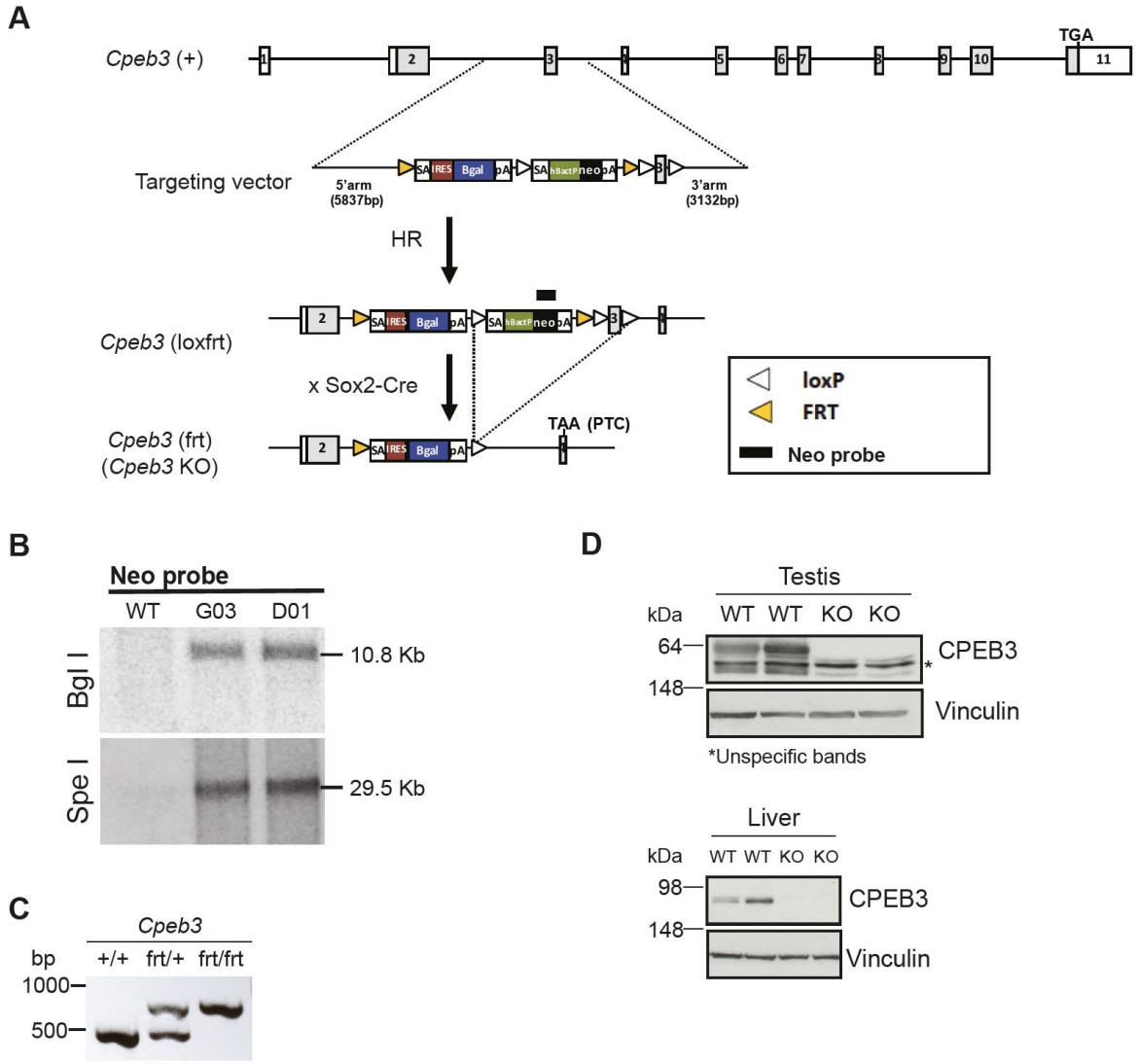

Supplementary Fig.3. Generation of CPEB3 KO mouse model. (A) Schematic representation of the targeting strategy followed and the alleles. Mouse *Cpeb3* locus contains 11 exons (boxes) including protein-coding (grey) and untranslated (clear) sequences. Recombinant ES cells harbouring one CPEB3loxfrt allele (clones HEPD0670_2_C02 and HEPD0670_2_G03; Eucomm) were obtained by homologous recombination (HR) with targeting vector PG00205_Z_3_F02 (Eucomm). CPEB3loxfrt allele carries a gene-trap lacZ cassette plus a promotor-DNA recombinases Cre and Flp, respectively. Excision of neo cassette and exon3 was achieved by crossing Cpeb3+/loxfrt mice with transgenic Sox2-Cre mice. The resulting Cpeb3frt allele includes a gene-trap lacZ cassette and a premature termination codon (PTC) and is considered a CPEB3 KO allele. hBactP, promotor. Bgal, β-galactosidase. Neo, neomycin. IRES, internal ribosome entry site. SA, splicing acceptor. pA, polyA sequence. (B) Southern blot of selected ES clones that underwent HR. DNA was digested with the indicated restriction enzymes and hybridized with a Neo probe. Images courtesy of Almudena Fernández, CIBERER-ISCIII at CNB-CSIC. (C) PCR amplification of WT (lower band) and FRT (upper band) Cpeb3 alleles. (D) Western blot detection of CPEB3 and Vinculin (control) in testis and liver protein extracts obtained from WT and CPEB3 KO mice.

Supplementary Fig. 4

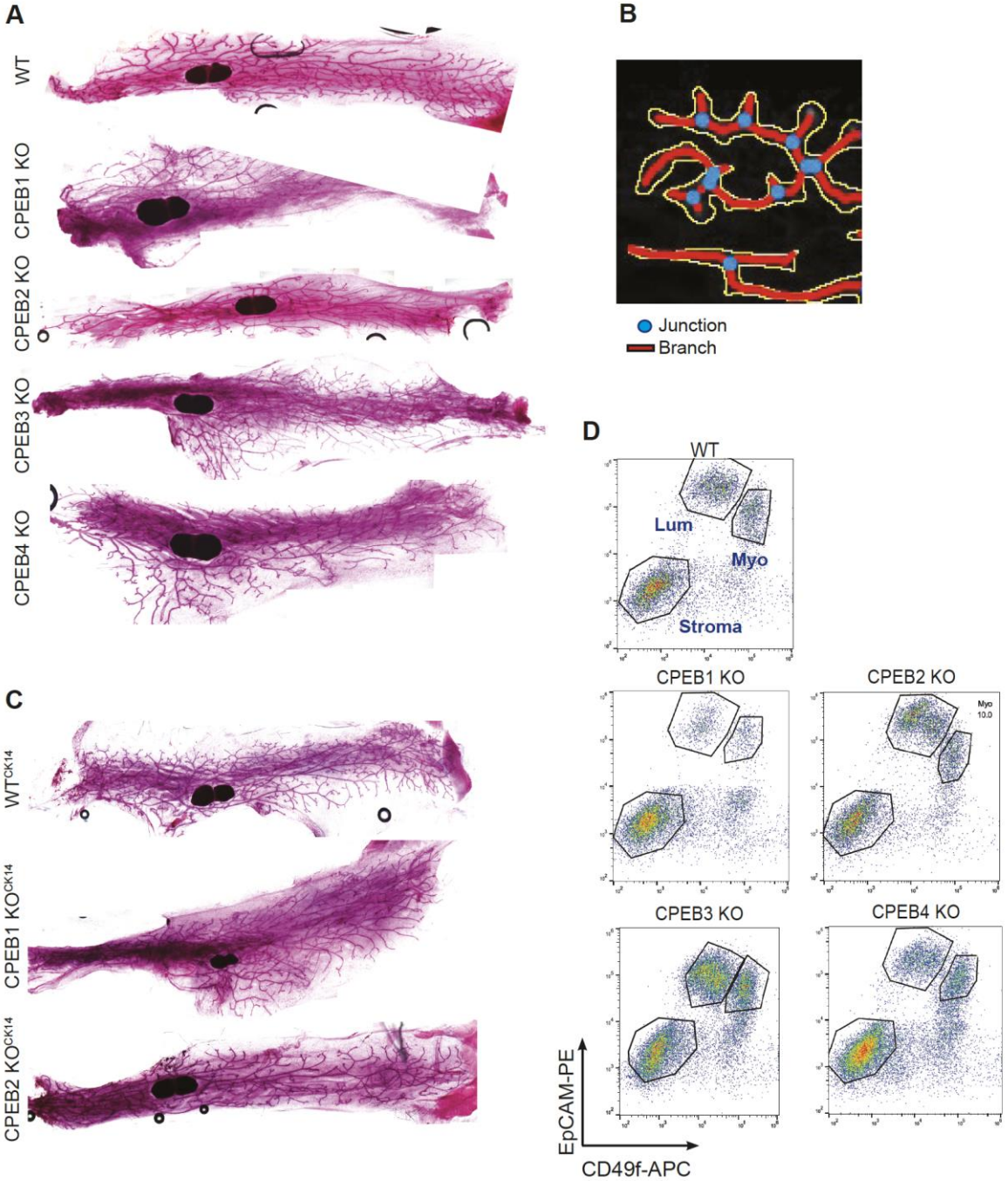

Supplementary Fig. 4. Mammary whole mounts and and FACS plots for CPEB1-4 KO models. (A) Example of an output image from AngioTool software (see Methods). (B) Whole images from the onsets shown in Fig.1C. (C) Whole images from the onsets shown in Fig.1D. (D) Representative FACS plots for the indicated genotypes gated on lineage negative cells. Lum, luminal ($EpCAM^{high}$ $CD49f^{low}$). Myo,myoepithelial ($EpCAM^{low}$ $CD49f^{high}$). Related to Fig.1F.

Supplementary Fig. 5

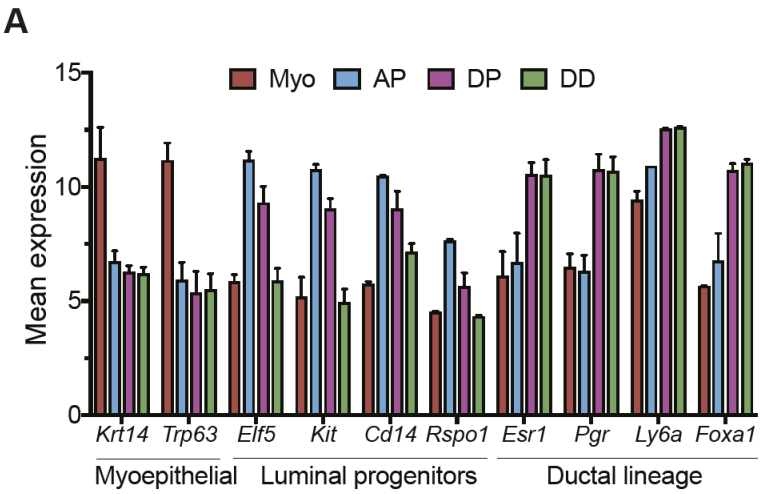

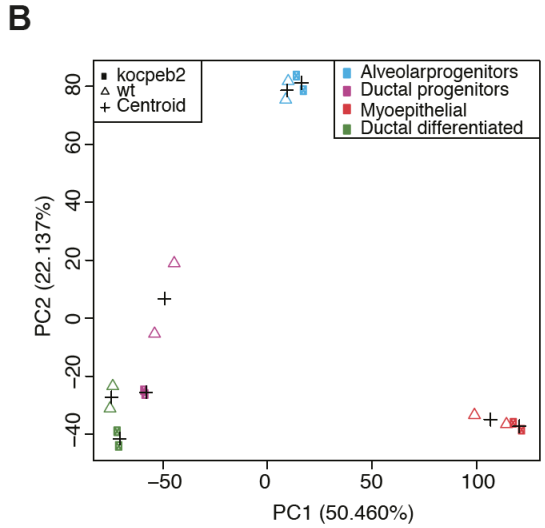

	Centroid distance
AP WT vs AP KO	63.25151048
DP WT vs DP KO	100.1056334
DD WT vs DD KO	83.76694453
Myo WT vs Myo KO	68.63573171

	Dispersion population
Alveolar progenitors	42.91
Ductal progenitors	60.11
Ductal differentiated	53.87
Myoepithelial	50.29

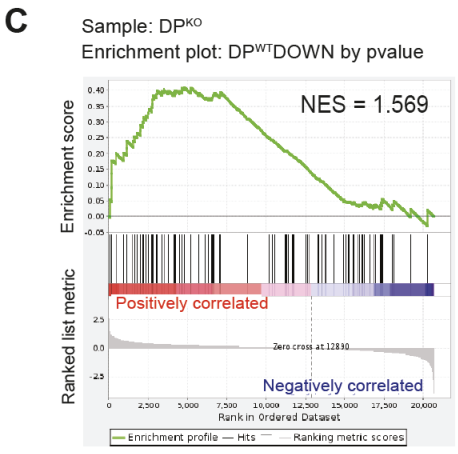

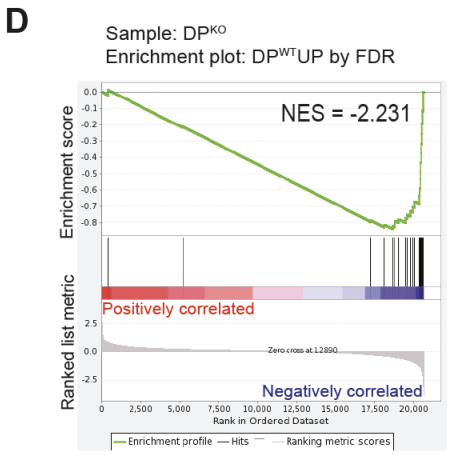

Supplementary Fig. 5. Microarray analysis for epithelial populations in WT and CPEB2-KO mice. (A) Mean expression of probes for markers of the various epithelial cell populations. (B) Principal Component Analysis (PCA) of the microarray hybridization results and the computed centroid distances and dispersion (see Methods). Pre-ranked GSEA graphical output for the enrichment in DP_{KO} of the DP_{WT}DOWN signature by p-value (C) or DP_{WT}UP signature by FDR (D). (C) and (D) FDR q-value=0.000. NES, normalized enriched score.

Supplementary Fig. 6

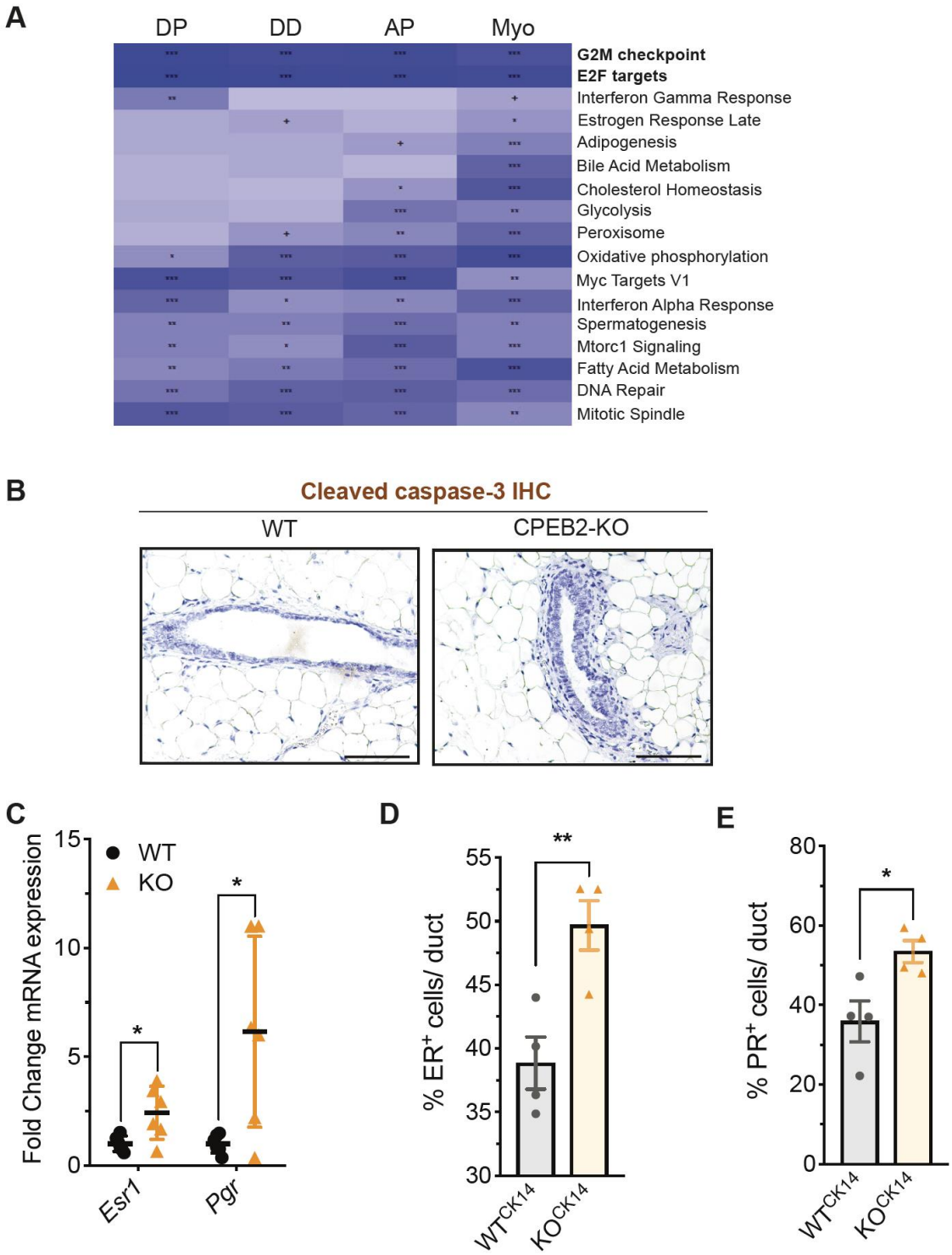

Supplementary Fig. 6. Proliferation in WT and CPEB2 KO mammary glands. (A) Heatmap illustrating expression changes from the microarray data. Specifically, hallmark gene sets (Broad Institute) downregulated in CPEB2 KO compared to WT are shown. FDR+/*/**/*** for 0.25/0.10/0.05/0.01. (B) Representative fields of cleaved caspase-3 staining in the adult mammary glands with the indicated genotype. Scale bar, 50 μm. (C) mRNA levels in total adult mammary gland tissue normalized to Gapdh and to WT value (*n*=6). *P < 0.05 b y two-tailed Student's t-test. (D) Automatic quantification of ER-positive in WT^{CK14} and KO^{CK14} mammary ducts (n=4). **P<0.01 by Mann-Whitney test. (E) Automatic quantification of PR-positive in WT^{CK14} and KO^{CK14} mammary ducts (n=4). **P<0.01 by Mann-Whitney test.

Supplementary Fig. 7

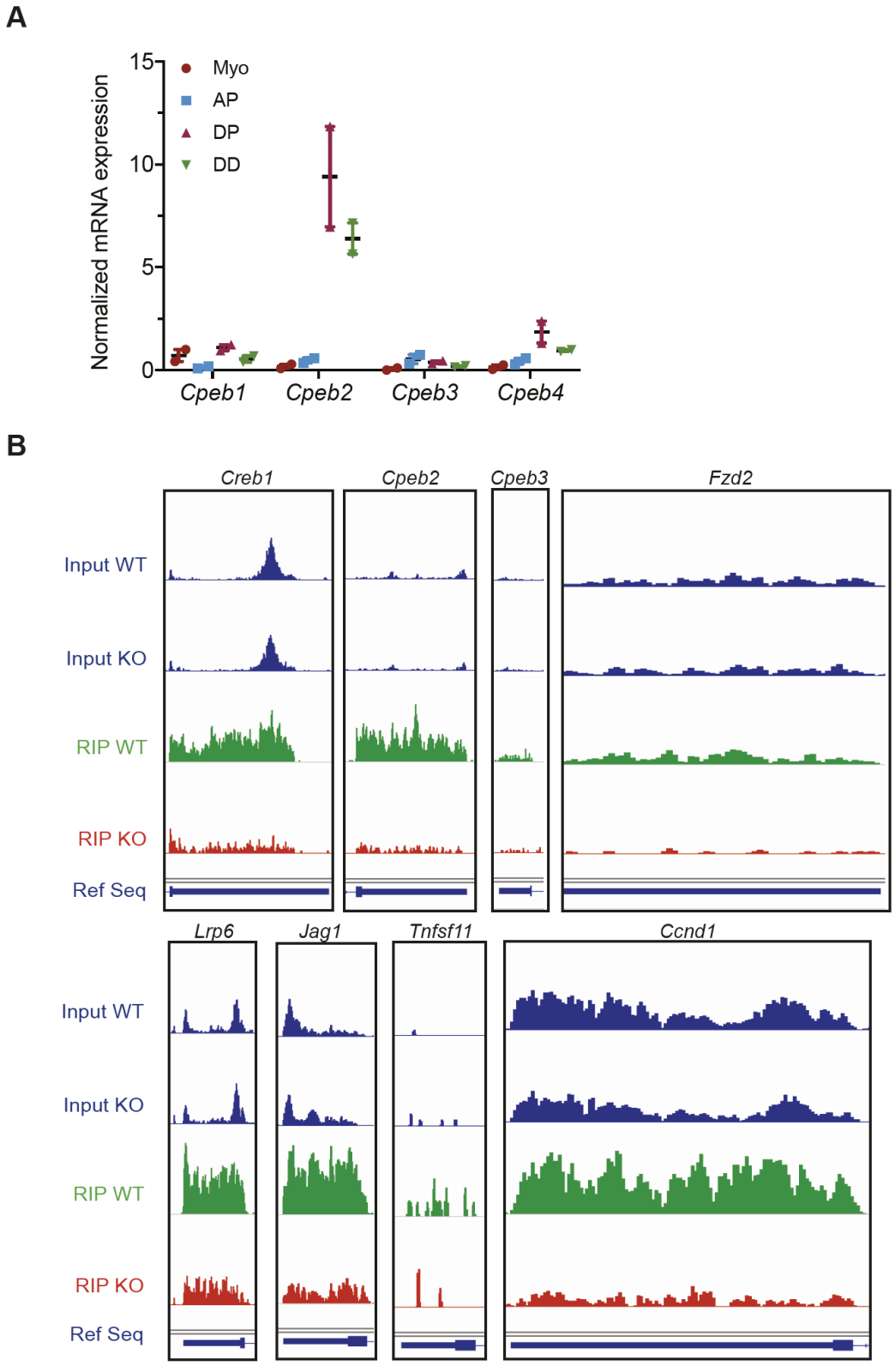

Supplementary Figure 7. Expression of CPEB1-4 in epithelial populations and RIP-Seq targets. (A) mRNA levels of the CPEB-family members in the different mammary epithelial subpopulation-s normalized by *Gapdh*. (B) Snapshots of RIP-Seq data for several 3'UTRs depicting normalized RIP-seq coverage for Inputs (blue), WT RIP (green) and KO RIP (red). Image obtained using the integrated genomic viewer (IGV). Data range: 0-7 arbitrary units for all 3'UTRs except for *Tnfsf11* (Rankl mRNA) (data range: 0-1 arbritary units).

Supplementary Fig. 8

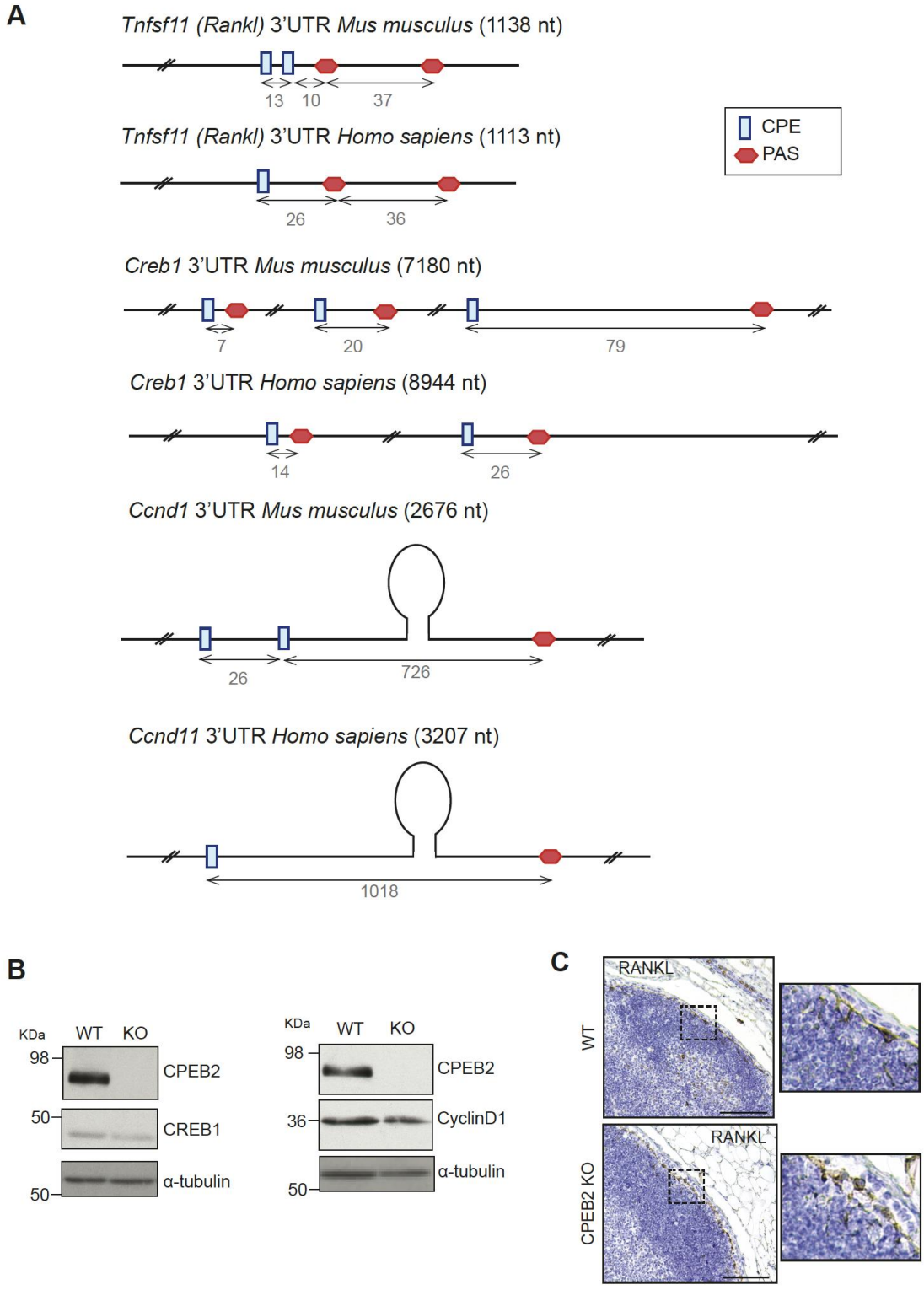

Supplementary Figure 8. CPEB2-targets in the MECs. (A) Schematic representation of selected 3′ UTRs in mouse and human. Canonical cytoplasmic polyadenylation elements (CPEs) and polyadenylation signals (PAS) are depicted, as well as the distance in nucleotides (nt) between these motifs. (B) Western blot image for CPEB2, CREB1, CyclinD1 and α-tubulin (loading control) in WT and KO MECs. (C) Representative images of RANKL-positive cells by IHC in lymph nodes, same samples as in Figure 4F are shown.

Supplementary Fig. 9

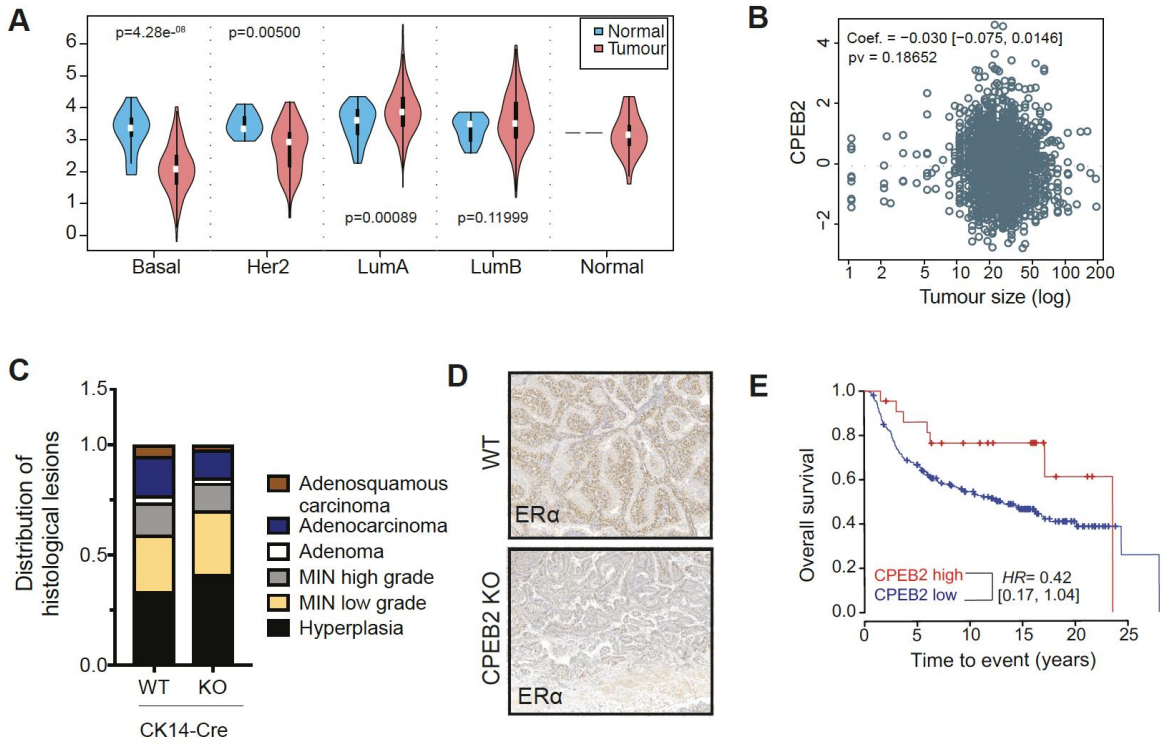

Supplementary Fig. 9. Extended data for CPEB2 and breast cancer. (A) Violin plots for mean RNA expression of CPEB2 in the PAM50 subtypes in tumour and adjacent normal tissue, analysis with TCGA dataset (Genomic Data Commons); P-values for Wald test indicated in the graph (n=860). (B) Association between tumour size and CPEB2 expression in Metabric dataset, Wald test (n=1954). (C) Distribution of histological lesions in WT^{CK14} (n=9) and CPEB2 KO^{CK14} (n=9) classified according to Annapolis nomenclature. MIN, mammary intra-epithelial neoplasia. (D) Images from ER-positive cells in WT^{CK14} and CPEB2 KO^{CK14} tumours. (E) Kaplan-Meier survival curves for Basal-like Bca patients. Statistics by Cox test; HR(< 10y) = 0.42; P = 0.03223; n = 228.

Supplementary Fig. 10

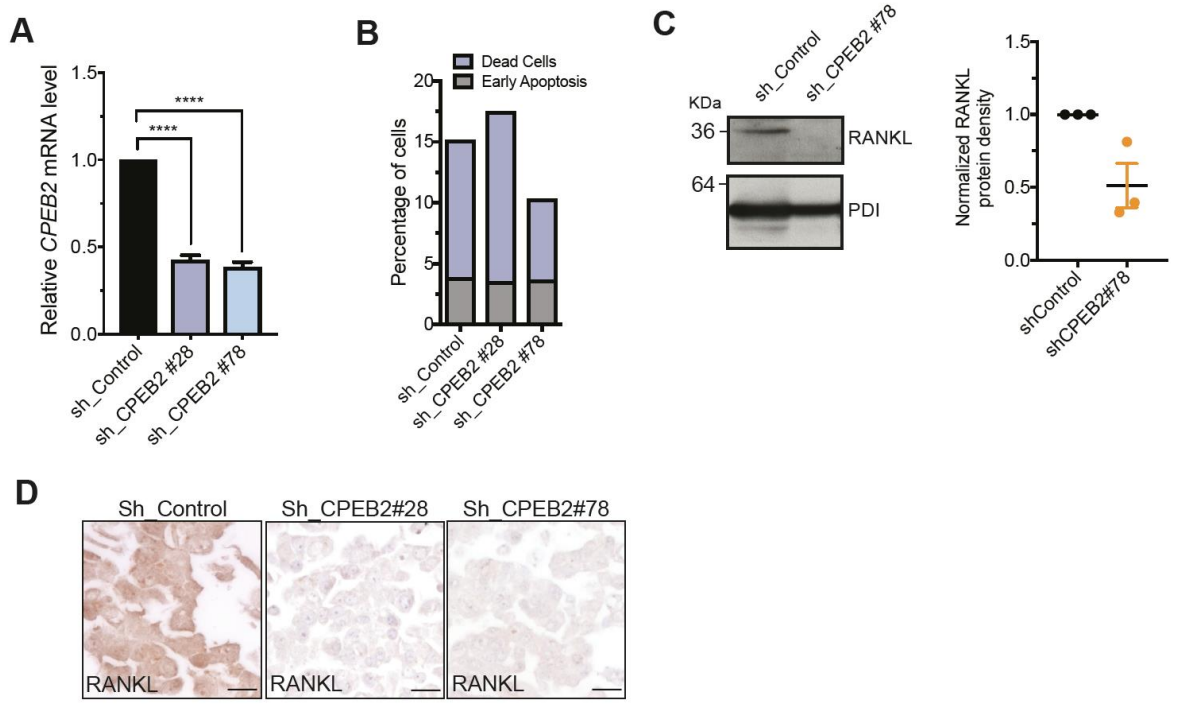

Supplementary Fig. 10. Characterization of CPEB2 KD cell lines. (A) Quantification of CPEB2 expression levels by RT-qPCR in ZR-75 cells infected with sh_Control, sh_CPEB2 #28 or #78 lentiviral plasmids to downregulate the expression of the gene. B2M was used as endogenous control. Statistics by two-tailed unpaired Student's t-test, ****P < 0.0001. (B) Percentage of early apoptotic Anexin V-positive cells (grey bars) and dead cells in 75 sh_Control, sh_CPEB2 downregulated cells. (C) Western blot imae for RANKL and PDI (an ER marker used as control) and normalized quantification in membrane-enriched lysates of ZR-75 cells infected with sh_Control, shCPEB2#28 or shCPEB2#78. (D) Images from RANKL IHC in cell pellets from ZR-75 cells infected with sh_Control, shCPEB2#28 or shCPEB2#78. Scale bar, 25 μm.

Supplementary Fig. 11

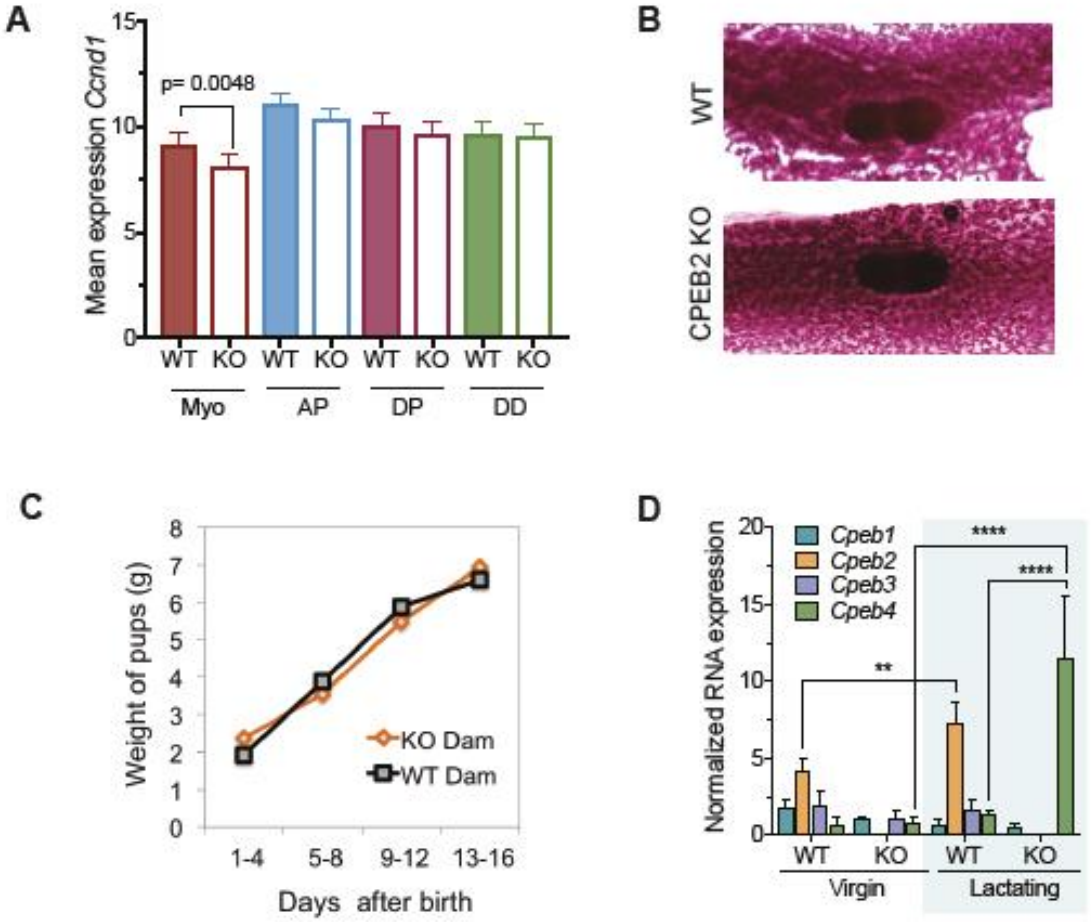

Supplementary Fig. 11. CPEB2 deficiency could be compensated by CPEB4 during lactation. (A) Mean mRNA expression of Ccnd1 in the epithelial subpopulations (microarray data in virgin mammary glands). (B) Mammary wholemounts from WT and CPEB2 KO females at mid-pregnancy. (C) Weight of heterozygous pups nursed by WT or CPEB2 KO dams. (D) mRNA levels of Cpeb1-4 normalized to Gapdh in whole mammary tissue in adult (n=7) or lactating (n=2) WT and CPEB2 KO females. Statistics by two-way ANOVA, **P < 0.01, ***P < 0.001. KO.